

# We are IntechOpen, the world's leading publisher of Open Access books Built by scientists, for scientists

5,500

Open access books available

136,000

International authors and editors

170M

Downloads

Our authors are among the

154

Countries delivered to

TOP 1%

most cited scientists

12.2%

Contributors from top 500 universities



WEB OF SCIENCE™

Selection of our books indexed in the Book Citation Index  
in Web of Science™ Core Collection (BKCI)

Interested in publishing with us?  
Contact [book.department@intechopen.com](mailto:book.department@intechopen.com)

Numbers displayed above are based on latest data collected.  
For more information visit [www.intechopen.com](http://www.intechopen.com)



# Analysis of Wideband Second-Order Microwave Integrators

*Usha Gautam and Tarun Kumar Rawat*

## Abstract

This chapter presents the implementation of stable, accurate, and wideband second-order microwave integrators (SOMIs). These SOMI designs are obtained by the use of various cascading combinations of transmission line sections and shunt stubs. In order to obtain the optimal values of the characteristic impedances of these line elements, the particle swarm optimization (PSO), cuckoo search algorithm (CSA) and gravitational search algorithm (GSA) are used to approximate the magnitude response of the ideal second-order integrator (SOI). Based on magnitude response, absolute magnitude error, phase response, convergence rate, pole-zero plot, and improvement graph, the performance measure criteria for the proposed SOMIs are performed. The results of the simulation and statistical analysis reveal that GSA exceeds the PSO and CSA in order to approximate the ideal SOI in all state-of-the-art eligible for wide-band microwave integrator. The designed SOMI is compact and suitable for applications covering ultra-wideband (UWB). The designed SOMI structure is also simulated on Advanced Design Software (ADS) in the form of a microstrip line on a dielectric constant 2.2 RT/Duroid substrate with a height of 0.762 mm. In the 3–15 GHz frequency range, the simulated magnitude result agrees well with the ideal one.

**Keywords:** Cuckoo search algorithm, gravitational search algorithm, particle swarm optimization, line elements, microwave integrator

## 1. Introduction

Integration plays an important role in many scientific and engineering applications. An integrator is an electronic circuit which produces the output that is the integral of the input applied. Electronic analogue integrators are the basis of analog computers and charge amplifiers, which are performed in the continuous time domain. The integrator is widely used in analog computers, analog-to-digital converters and wave-shaping circuits. Initially, an RC integrator is a circuit that approximates the mathematical process of integration. A simple R-C integrator circuit is shown in **Figure 1**, in which a capacitor (C) in series with a resistor (R) and the source ( $V_{in}$ ). The output ( $V_{out}$ ) of the circuit is taken across the capacitor (C).

Let  $i$  is the resulting current. Applying Kirchhoff's voltage law to the circuit,

$$V_{in} = iR + \frac{1}{C} \int_0^t i \cdot dt \quad (1)$$

$$V_{out} = \frac{1}{C} \int_0^t i \cdot dt \quad (2)$$

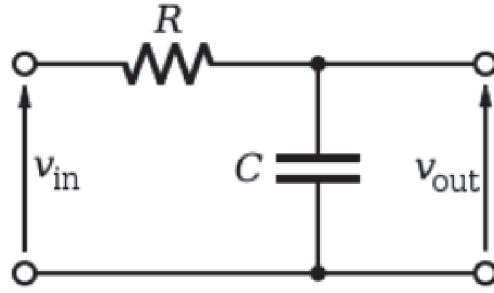


**Figure 1.**  
R-C Integrator circuit.

Multiplying throughout by C, we get

$$CV_{in} = iRC + \int_0^t i \cdot dt \quad (3)$$

as  $RC \gg t$ , the term  $\int_0^t i \cdot dt$  may be neglected

$$CV_{in} = iRC \quad (4)$$

Integrating with respect to  $t$  on both sides of Eq. (3)

$$\int_0^t CV_{in} = RC \int_0^t i \cdot dt \quad (5)$$

$$\frac{1}{C} \int_0^t i \cdot dt = \frac{1}{RC} \int_0^t V_{in} \cdot dt \quad (6)$$

From Eq. (2),

$$V_{out} = \frac{1}{RC} \int_0^t V_{in} \cdot dt \quad (7)$$

Eq. (7) shows that the output of an integrator circuit is the integral of the input signal. These analog integrators are limited for low frequency application. Thus, the researcher moved to design digital integrators. Digital integrator is a system that performs mathematical operations on a sampled discrete time signal to reduce or enhance certain aspects of that signal. It is commonly used for applications such as waveform shaping, coherent detection, edge detection, and accumulator analysis in biomedical engineering and signal processing. It is widely utilized in biomedical engineering and signal processing applications, for example, as waveform shaping, coherent detection, edge detection, and accumulator analysis. It is also used in radar applications such as the allocation of mobile satellites, enterprise networks, commercial television services and digital services [1]. In order to design the wideband digital integrators, various methods were intended. Using the Newton-cotes integration rule and various digital integration techniques, the Recursive wideband digital integrators have been designed [2]. For low-speed applications up to barely a few hundred MHz, the integrators are primarily designed and implemented. Therefore, to cover wideband applications such as radar and wireless communication, the design and implementation of integrators for high-frequency applications is necessary. The microwave integrator is essentially used to measure the time integral of the input signal at microwave frequencies (0.3–300 GHz). Using wideband integrators, the high-frequency active filters can be introduced, and these wideband integrators can also be used for industrial and real-time applications for

ultra-wideband (frequency range 3.1–10.6 GHz) applications [3–5]. In the z-domain, Hsue et al. have introduced a first-order trapezoidal-rule microwave integrator using a chain-scattering transmission matrix with an operating frequency range from 1 to 10 GHz [6]. By cascading equal-length transmission line sections in the z-domain, three microwave integrators and differentiators have been designed and implemented with different time constants [7, 8]. The second-order microwave integrator (SOMI) was designed by Tsai et al. [9] in the z-domain. A further first-order microwave integrator was designed by Gautam et al. using the ABCD transmission matrix with a bandwidth of 4 to 10 GHz [10]. SOMI was designed by Gupta et al. in the z-domain over the 1.5–5.5 GHz frequency range [11]. Another SOMI was designed by Gautam et al. in the z-domain over the frequency range 3–15 GHz [12]. Nowadays, analyzers are gravitating towards the use of population-based meta-heuristic algorithms to optimize system coefficients in order to design complex or multi-modal systems [13–17]. This chapter introduces modern and compact SOMI designs that lead to wide bandwidth. These designed SOMIs are accomplished by cascading three transmission line sections and two single section stubs of equal length. By population-based meta heuristic algorithms, the optimum value of characteristic impedances of these line elements are obtained. A global cost-function solution is achieved by minimizing the error gap between the ideal second-order integrator (SOI) and the designed SOMIs. The design-1 SOMI approximates the ideal SOI over the 2.5 to 16 GHz frequency range, and the design-2 SOMI approximates the ideal SOI over the 3 to 15 GHz frequency range. These designed wideband SOMIs would operate with a wider frequency band to be used in mobile communication on a mobile network such as 4 G and 5 G (above 3 GHz) [18]. All the simulated results are obtained by MATLAB and ADS. These simulated outcomes are formulated to be in close agreement with the ideal one. The novelty of these designed SOMIs exists in terms of wide bandwidth and miniaturization of hardware.

## 2. Problem formulation of SOMIs

To realize second-order microwave integrator in microwave range, consider a two-port network, which is illustrated in **Figure 2**.

Its scattering matrix is defined as [4].

$$\begin{bmatrix} b_1 \\ b_2 \end{bmatrix} = \begin{bmatrix} S_{11} & S_{12} \\ S_{21} & S_{22} \end{bmatrix} \begin{bmatrix} a_1 \\ a_2 \end{bmatrix} \quad (8)$$

where  $a_1$  and  $a_2$  are incident waves at port 1 and port 2, respectively, and  $b_1$  and  $b_2$  are reflected waves at port 1 and port 2, respectively [4]. The chain scattering matrix of a two-port network can be established from the scattering matrix (S-matrix). The chain-scattering matrix of two-port network is defined as [5].

$$\begin{bmatrix} a_1 \\ b_1 \end{bmatrix} = \begin{bmatrix} T_{11} & T_{12} \\ T_{21} & T_{22} \end{bmatrix} \begin{bmatrix} b_2 \\ a_2 \end{bmatrix} \quad (9)$$

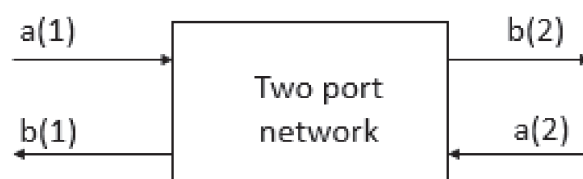


**Figure 2.**  
*Two-port network.*

For network computation the chain-scattering matrix from S-matrix (on solving Eq. (8) and Eq. (9))

$$T_{11} = \frac{1}{S_{21}}$$

$$T_{12} = -\frac{S_{22}}{S_{21}}$$

$$T_{21} = \frac{S_{11}}{S_{21}}$$

$$T_{22} = \frac{S_{12} S_{21} - S_{11} S_{22}}{S_{21}}$$

Then the chain-scattering matrix is

$$\begin{bmatrix} T_{11} & T_{12} \\ T_{21} & T_{22} \end{bmatrix} = \begin{bmatrix} \frac{1}{S_{21}} & -\frac{S_{22}}{S_{21}} \\ \frac{S_{11}}{S_{21}} & \frac{S_{12} S_{21} - S_{11} S_{22}}{S_{21}} \end{bmatrix} \quad (10)$$

The formulation of SOMIs is employed with equal length line elements is cascading. The overall transfer function of a cascaded network can be established by multiplying the chain scattering matrices of the line elements. These line elements can be transmission line sections and stubs. Assume the length of all transmission line sections and stubs is  $l = \lambda_o/4$ , where  $\lambda_o$  represents the wavelength of the lines at the normalizing angular frequency or we can say that the electrical length of each section (stubs and transmission lines) is set to be  $90^\circ$  at the normalizing frequency. The electrical length of line element is  $\theta = \beta l$ .

The frequency response of an ideal second order integrator (SOI) is given by

$$H(j\omega) = \frac{1}{\omega^2} \quad (11)$$

where  $\omega$  represents the angular frequency in radians per second. Since the magnitude response of an open-circuited stub decreases with frequency, an open-circuited stub can be chosen to design an integrator. Assume the impedance of an open-circuited stub to be  $Z_{oc}$ . Its chain scattering is [5].

$$\begin{bmatrix} T_{11} & T_{12} \\ T_{21} & T_{22} \end{bmatrix}_{open} = \begin{bmatrix} 1 + j \frac{Z_0}{2Z_{oc}} \tan(\beta l) & j \frac{Z_0}{2Z_{oc}} \tan(\beta l) \\ -j \frac{Z_0}{2Z_{oc}} \tan(\beta l) & 1 - j \frac{Z_0}{2Z_{oc}} \tan(\beta l) \end{bmatrix} \quad (12)$$

where  $Z_0$  represents the reference characteristic impedance that is  $50 \Omega$ ,  $Z_{oc}$  is the characteristic impedance of an open circuited stub and  $\beta$  represents the phase constant.

Assume  $\omega$  is the angular frequency and  $\tau$  is the propagation delay attributable to the length  $l$ . Therefore, the term  $j \tan(\beta l) = j \tan(\omega\tau)$  can be expressed by  $D^{-1} = e^{-j\omega\tau}$ , which can be considered as a unit of delay, that is [5].

$$j \tan(\omega\tau) = \frac{e^{j\omega\tau} - e^{-j\omega\tau}}{e^{j\omega\tau} + e^{-j\omega\tau}} = \frac{D - D^{-1}}{D + D^{-1}} \quad (13)$$

Subsequently, the chain scattering matrix of open-circuited stub is

$$\begin{bmatrix} T_{11} & T_{12} \\ T_{21} & T_{22} \end{bmatrix}_{open} = \frac{1}{1 + D^{-2}} \begin{bmatrix} (1 + k) + (1 - k)D^{-2} & (k - kD^{-2}) \\ -k + kD^{-2} & (1 - k) + (1 + k)D^{-2} \end{bmatrix} \quad (14)$$

where  $k = \frac{Z_0}{2Z_{oc}}$ . Now we substitute  $z = D^2$  in above Eq. (14) for designing purpose, which resembles a scaling by two on frequency axis. Then the chain scattering matrix of open-circuited stub is [6].

$$\begin{bmatrix} T_{11} & T_{12} \\ T_{21} & T_{22} \end{bmatrix}_{open} = \frac{1}{1 + z^{-1}} \begin{bmatrix} (1 + k) + (1 - k)z^{-1} & (k - kz^{-1}) \\ -k + kz^{-1} & (1 - k) + (1 + k)z^{-1} \end{bmatrix} \quad (15)$$

and  $S_{21}$  is given by

$$S_{21} = \frac{1}{T_{11}} = \frac{1 + z^{-1}}{(1 + k) + (1 - k)z^{-1}} \quad (16)$$

where  $z = e^{j\beta l}$ . Likewise, the chain scattering matrix for the transmission line section in  $Z$  domain is given by [6].

$$\begin{bmatrix} T_{11} & T_{12} \\ T_{21} & T_{22} \end{bmatrix}_{TLS} = \frac{1}{z^{-\frac{1}{2}}(1 - \Gamma^2)} \begin{bmatrix} 1 - \Gamma^2 z^{-1} & -\Gamma - \Gamma z^{-1} \\ 1 - \Gamma z^{-1} & -\Gamma^2 + z^{-1} \end{bmatrix} \quad (17)$$

where the reflection coefficient  $\Gamma$  is given by

$$\Gamma = \frac{Z_{TL} - Z_0}{Z_{TL} + Z_0} \quad (18)$$

where  $Z_{TL}$  represents the characteristic impedance of serial transmission line section. Similarly, the chain scattering matrix of a short-circuited stub is given by [8]

$$\begin{bmatrix} T_{11} & T_{12} \\ T_{21} & T_{22} \end{bmatrix}_{Short} = \frac{1}{1 - z^{-1}} \begin{bmatrix} (1 + \delta) - (1 - \delta)z^{-1} & (\delta + \delta z^{-1}) \\ -\delta - \delta z^{-1} & (1 - \delta) - (1 + \delta)z^{-1} \end{bmatrix} \quad (19)$$

where the coefficient  $\delta$  is given by

$$\delta = \frac{Z_0}{2Z_{SC}} \quad (20)$$

where  $Z_{SC}$  represents the characteristic impedance of the short-circuited stub. Serial line sections and short-circuited stubs shunted with open circuited stub should be employed in the transmission line configuration to design an integrator by cascading. A cascaded connection of two-port network is equivalent to a single two-port network containing a product of matrices. Assume the SOI is composed of  $P$  open-circuited stubs,  $Q$  short-circuited stubs and  $R$  transmission line sections. The overall  $S_{21}$  in generalized form is given by

$$S_{21} = \frac{1}{T_{11}} = \frac{(1 + z^{-1})^P (1 - z^{-1})^Q z^{-R/2} \prod_{r=1}^R (1 - \Gamma_r^2)}{\alpha_0 + \alpha_1 z^{-1} + \alpha_2 z^{-2} + \alpha_3 z^{-3} + \dots + \alpha_N z^{-N}} \quad (21)$$

where,  $P$  denotes the number of open-circuited stubs,  $Q$  denotes the number of short-circuited stubs,  $R$  denotes the number of transmission line section,  $N$  is the total number of line elements  $N = P + Q + R$  and  $\alpha_o, \alpha_1, \alpha_2, \dots, \alpha_N$  Coefficients are functions of the reflection coefficient of each section of the transmission line and stub characteristic impedances (in terms of open-circuited stub coefficient  $k$  and short-circuited stub coefficient  $\delta$ ). In addition, to design the SOMI, serial transmission lines cascaded with shunt circuited stubs can be employed. Then the frequency-domain response of the transfer function, which has an integrator characteristic, is thus obtained. In order to design a wideband SOMI, the following two methods are used.

Design-I (SOMI using two open stubs and three transmission line sections): In this design, we may select two open-circuited stubs and three transmission line sections as shown in **Figure 3**, where  $P = 2, R = 3$ . Overall  $S_{21}$  of the design-1 SOMI is given by

$$S_{21} = \frac{(1 + z^{-1})^2 z^{-3/2} \prod_{r=1}^3 (1 - \Gamma_r^2)}{\alpha_o + \alpha_1 z^{-1} + \alpha_2 z^{-2} + \alpha_3 z^{-3} + \alpha_4 z^{-4} + \alpha_5 z^{-5}} \quad (22)$$

Design-II (SOMI using one open stub, one short stub and three transmission line section): In this design, a short-circuited stub is cascaded with the transmission line sections and an open-circuited stub as shown in **Figure 5**, where  $P = 1, Q = 1, R = 3$ . Overall  $S_{21}$  of the design-2 SOMI is given by

$$S_{21} = \frac{(1 - z^{-2}) z^{-3/2} \prod_{r=1}^3 (1 - \Gamma_r^2)}{\alpha_o + \alpha_1 z^{-1} + \alpha_2 z^{-2} + \alpha_3 z^{-3} + \alpha_4 z^{-4} + \alpha_5 z^{-5}} \quad (23)$$

The term  $(1 + z^{-1})$  is due to open-circuited stub, the term  $(1 - z^{-1})$  is due to short-circuited stub, and  $z^{-3/2}$  is the delay factor of the transmission line section. These line elements are transmission lines of equal length with a length of  $l = \lambda_0/4$  at an operating frequency of 12.5 GHz.

The next task be to achieve the optimum value of characteristic impedances of design-1 and design-2 SOMI line elements. The optimization algorithms are used to obtain these characteristic impedances of the line elements. In order to lower the cost function, the design of SOMI is considered as an approximation problem. The cost function differs between the response in magnitude of an ideal SOI and the SOMI designed. The cost function is formulated in the sense of least squares and can be expressed as

$$CF = \min \int_0^\pi |E(\omega)|^2 d\omega = \min \int_0^\pi |H(\omega) - S_{21}|^2 d\omega \quad (24)$$

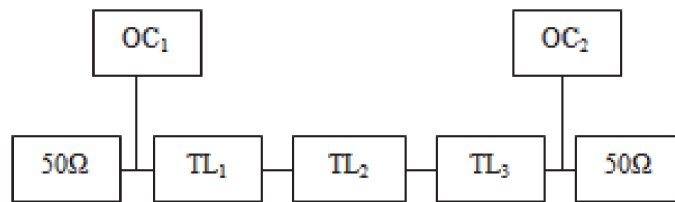


**Figure 3.**  
Configuration of the design-1 SOMI.

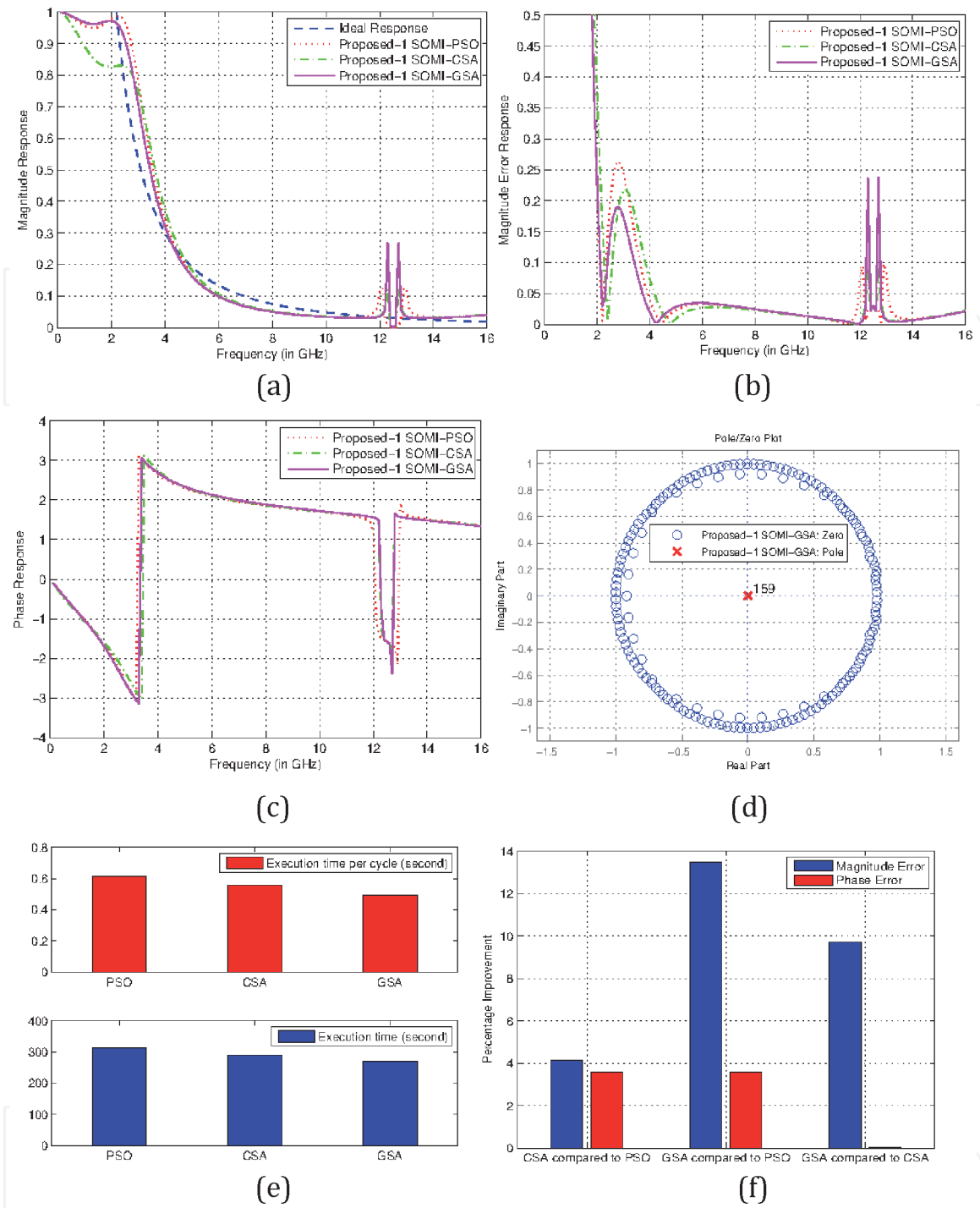


**Figure 4.** Profile of design-1 SOMI (a) Magnitude response, (b) Magnitude error response, (c) Phase response, (d) Pole-zero plot, (e) Convergence profile, and (f) Improvement bar-graph.

where  $E(\omega) = (H(\omega) - S_{21})$  is the cost function, in which  $H(\omega)$  is the frequency response of an ideal SOI.

### 3. Employed optimization methods

In infinite impulse response (IIR) systems, the error surface is generally non-quadratic and multimodal with respect to the system parameters. Minimization of such error fitness function using derivative-based search algorithm is difficult. This is due to the fact that the derivative-based search algorithm may not converge to the global minima and get stuck in local minima. Moreover, IIR systems are associated



with the stability issues as the poles of the systems may lie outside the unit circle. Such techniques are found unfit to solve multi-objective, multi-modal complex problems and a fine tuning of algorithm parameters is required. To conquer these disadvantages, several practitioners rely on meta-heuristic algorithms, which are based on natural evolution. The meta-heuristic algorithms are nature inspired population-based search techniques which have the ability to serve a global optimal solution with high convergence by accumulating random search and selection principle. Therefore, intelligent search paradigms and optimization methods are adopted in this work for an optimal differentiator design (a multi-modal problem) in short computation time and with high accuracy. Three population-based heuristic search algorithms PSO, CSA, and GSA are employed in this section to diminish the cost function in order to find optimum values of characteristic impedances for designed wideband SOMIs of line elements. **Table 1** displays the optimum set of algorithm control parameters for designed SOMIs. A brief description of all three algorithm is discussed below.

### 3.1 Particle swarm optimization

Particle swarm optimization was proposed by Kennedy and Eberhart in nineties based on swarm behavior. PSO has simplicity, high solution quality and superior convergence characteristics as compared to other algorithms. It is more efficient, easy to implement and flexible to control between global and local exploration of the search space [13, 14]. In PSO, every particle has a candidate solution and each candidate solution has its position and velocity. The position vector gives the required solution and the velocity vector gives the current position by which it reaches at the new position. After every iteration, the position and the velocity vectors are updated unless final coefficients are obtained. The velocity and position vector are updated according to the following equations:

Parameters	PSO	CSA	GSA
Population size	$n_p = 25$	$n_c = 25$	$n_g = 25$
Maximum Iteration	400	400	400
$C_1$	2	—	—
$C_2$	2	—	—
$v_i^{min}$	0.01	—	—
$v_i^{max}$	1.0	—	—
$w_{min}$	0.1	—	—
$w_{max}$	1.0	—	—
Discovering rate of alien egg, Pa	—	0.25	—
$G_0$	—	—	100
$\alpha$	—	—	20
$\epsilon$	—	—	0.001
$r^{Norm}$	—	—	2
$r^{Power}$	—	—	1

**Table 1.**  
Control parameters of PSO, CSA and GSA for optimization.

$$v_i^{(k+1)} = \omega * v_i^{(k)} + C_1 * rand1 * (gbest_i^{(k)} - p_i^{(k)}) + C_2 * rand2 * (pbest_i^{(k)} - p_i^{(k)}) \quad (25)$$

$$p_i^{(k+1)} = p_i^{(k)} + v_i^{(k+1)} \quad (26)$$

where,  $v_i^k$  is the velocity of the  $i$ th particle and  $\omega$  is the weight factor.  $C_1$  and  $C_2$  are positive cognitive parameters while  $rand1$  and  $rand2$  are two random parameters has range from  $[0, 1]$ .  $gbest^k$  is the global best position component at  $k$ th iteration and  $pbest_i^{(k)}$  is the particular best value of  $i$ th particle.  $p_i^{(k)}$  is the position vector of  $i$ th particle at  $k$ th iteration. Some parameters are selected to obtain the characteristic impedances of line elements, which are provided in **Table 1**.

### 3.2 Cuckoo search algorithm

The cuckoo search algorithm is developed by Yang and Deb in 2009 which is inspired by the concept of unique breeding behavior of cuckoo bird in combination with Lévy ( $\lambda$ ) flights. The theoretical concepts of CSA are well developed and tested in [15–17]. The single parameter setting in CSA is proven to be a crucial superiority factor as compared to other nature-based algorithms. As a result, the optimized results are executed in very less time. CSA is employed in this section for determining the optimum characteristic values of impedances of transmission line elements on account of minimizing the magnitude error of designed SOMI.

The species of cuckoo birds lay eggs in other bird nests, where the host birds either throw off the detected strange eggs or leave their nests and move into a new spot. The algorithm symbolizes each host nest to a capable solution for this design problem and assigns it a fitness value, as defined in Eq. (24). Furthermore, CSA starts to exchange the current fitness value with a better solution iteratively. The concept of Lévy flights is then introduced in the process for exploration of new solutions, mathematically modelled using the Lévy distribution,  $1 < \lambda \leq 3$  [17] with an infinite variance and infinite mean.

### 3.3 Gravitational search algorithm

This algorithm is based on Newton's theory of gravitational force and was introduced by E Rashedi et al. in 2009 [19]. Candidates in GSA are supposed to be objects with a given mass. In accordance with Newton's Law, every candidate in a space has an attraction force with every other candidate. This force correlates inversely to the square of the distance between the candidates and is directly proportional to the product of their masses [20, 21]. Each candidate in the GSA has certain parameters: position of candidate's mass, inertial mass of candidate, active gravitational mass and passive gravitational mass between candidates. The position of the mass of candidates resembles the solution of the problem devised [21]. The gravitational mass and inertial mass are determined using a cost function of designed problem. The mathematical representation of GSA is considering  $N$  candidates within a system and all candidates are randomly positioned in search space. The gravitational force on candidate  $i$  from candidate  $j$  at time  $t$  in dimension  $d$  is defined as [19].

$$F_{ij}^{d(t)} = G^{(t)} \frac{M_{pi}^{(t)} \times M_{aj}^{(t)}}{R_{ij}^{(t)} + \epsilon} (x_j^{d(t)} - x_i^{d(t)}) \quad (27)$$

where,  $G^{(t)}$  represents gravitational constant at time  $t$ ,  $M_{pi}^{(t)}$  represents the passive gravitational mass related to candidate  $i$ ,  $M_{aj}^{(t)}$  represents the active gravitational mass related to candidate  $j$ ,  $R_{ij}^{(t)}$  represents the Euclidian distance between two candidates  $i$  and  $j$  and  $\varepsilon$  is a small constant. Then  $G^{(t)}$  is calculated as [19].

$$G^{(t)} = G_0 \times \exp(-\alpha \times itr / maxitr) \quad (28)$$

where,  $G_0$  represents the initial value of gravitation constant,  $\alpha$  is descending coefficient, the current iteration is represented by  $itr$ , and  $maxitr$  represents the maximum number of iterations.

Then the total force that acts on candidate  $i$  in dimension  $d$  is calculated as

$$F_i^{d(t)} = \sum_{j=1, j \neq i}^N rand_j F_{ij}^{d(t)} \quad (29)$$

where  $rand_j$  is a random number. As reported to the motion's law, the acceleration of candidate  $i$  is given as

$$acc_i^{d(t)} = \frac{F_i^{d(t)}}{Ma_{ii}^{(t)}} \quad (30)$$

where  $Ma_{ii}$  represents the mass of the candidate  $i$ . The inertial mass and the gravitational mass are updated as follows [19].

$$m_i^{(t)} = \frac{CF_i^{(t)} - worst^{(t)}}{best^{(t)} - worst^{(t)}} \quad (31)$$

where  $CF$  represents the cost function of the candidate  $i$ .

$$M_{pi}^{(t)} = \frac{m_i^{(t)}}{\sum_{j=1}^J m_j^{(t)}} \quad (32)$$

The best and worst value are given by

$$best^{(t)} = \min_{j \in (1..J)} CF_j^{(t)} \quad (33)$$

$$worst^{(t)} = \max_{j \in (1..J)} CF_j^{(t)} \quad (34)$$

Then the position and the velocity of candidates are given by [19].

$$position : x_i^{d(t+1)} = x_i^{d(t)} + v_i^{d(t+1)} \quad (35)$$

$$velocity : v_i^{d(t+1)} = rand_i \times v_i^{d(t)} + acc_i^{d(t)} \quad (36)$$

where  $rand_i$  represents a random number. Finally, the position and velocity of the candidate are obtained.

<b>Algorithm 1</b>
Pseudo code for GSA for the design of SOMI-GSA
Define $H(\omega)$ and fitness function, Eq. (24)
Initialize population size of candidates, $n_g$ and other control parameters
Set upper and lower bounds, maximum iterations, generate population
While iteration, $l$ increases, $N < 400$ do
Compute fitness using Eq. (24)
Evaluate gravitational constant, $G_0$ and $g_{best}$
Compute masses, gravitational forces, and acceleration using Eqs. (27)–(32). for each candidate
Update the velocity and position of each candidate using Eqs. (35), (36)
For minimization,
If $E^{l+1} < E^l$
New solutions are updated
EndIf
EndWhile
Record the best solution
Characteristic impedances optimized

## 4. Simulation results

In this section, simulation results are discussed and analyzed. All the simulation results are carried out in MATLAB environment. The same control parameters for PSO, CSA and GSA have been selected for appropriate comparison of optimization algorithms. The lower and upper limits of the optimized coefficients are set to be 10 and 150 for functional realizability. Absolute magnitude error (AME), phase response, pole-zero plot, convergence rate and improvement rate are taken into account in assessing the performance of the proposed SOMI magnitude response.

### 4.1 Design-1 [SOMI using two open stub and three serial line sections]

**Figure 3** presents the configuration of the design-1 SOMI, and **Table 2** displays the characteristic impedances of design-1 SOMI achieved with PSO, CSA and GSA. The algorithm steps have shown in section-3 by which these characteristic impedances are attained. The magnitude response, the AME, the phase response, the pole-zero plot, the fitness rate and the improvement graph are the parameters selected in **Figure 4(a)–(f)** for the frequency response analysis of the design-1 SOMI. **Table 3**

Characteristic impedance	PSO	CSA	GSA
$Z_{oc1}$	12	112.2	148.8
$Z_{TL1}$	49	17	10
$Z_{TL2}$	120	114	149
$Z_{TL3}$	14	11	43
$Z_{oc2}$	115	14	21

**Table 2.**  
 Optimized characteristic impedances of the design-1 SOMI.

Algorithm	Total magnitude error	Phase error
PSO	5.7746	1.0403
CSA	5.5353	1.0031
GSA	4.9954	1.0030

**Table 3.**  
Comparison summary of total magnitude and phase error for design-1 SOMI.

records the overall magnitude error and the phase error. **Table 4** and **Table 5** summarize the statistical analysis and the qualitatively analyzed data of magnitude error of the design-1 SOMI. It is observed that GSA-based results have least values in all aspects with respect to PSO and CSA. The pole-zero plot of the Design-1 SOMI for stability analysis in which all the poles and zeros lie inside the unit circle is shown in **Figure 4(d)**. This plot asserts that the SOMI design-1 is stable. The convergence profile of all three algorithms in which GSA is clearly demonstrated to be faster than PSO and CSA in less execution time is shown in **Figure 4(e)**, which is also summarized in **Table 6**. The percentage improvement comparison in magnitude error for the design-1 SOMI as CSA to PSO, GSA to PSO, and GSA to CSA and the percentage improvement comparison in phase errors summarized in **Table 7** are shown in **Figure 4(f)**. The design-1 SOMI GSA-based magnitude response closely matches that of the ideal one in the 2.5–16 GHz frequency range. On the basis of these observations, compared to the PSO and CSA, GSA has the lowest magnitude error and the highest convergence speed.

Algorithm	Mean	Variance	Standard deviation
PSO	0.0410	0.0035	0.0588
CSA	0.0393	0.0036	0.0603
GSA	0.0354	0.0024	0.0494

**Table 4.**  
Statistical data of magnitude error for design-1 SOMI.

Algorithm	Maximum	Minimum	Average
PSO	0.2642	$4.8442 \times 10^{-4}$	0.0410
CSA	0.3762	$9.2306 \times 10^{-4}$	0.0393
GSA	0.2384	$4.2118 \times 10^{-4}$	0.0354

**Table 5.**  
Qualitatively data of magnitude error for design-1 SOMI.

Algorithm	Iteration cycle	Execution time (s) per iteration	Execution time (s) per cycle
PSO	400	313.2654	0.6132
CSA	400	291.3719	0.5547
GSA	400	269.6370	0.4950

**Table 6.**  
Convergence profile for design-1 SOMI.

Algorithm	Magnitude PI (%)	Phase PI (%)
PSO	4.1613	3.5758
CSA	13.4935	3.5855
GSA	9.7374	0.0099

**Table 7.**  
 Percentage improvement in magnitude and phase error for design-1 SOMI.

#### 4.2 Design-2 [SOMI using one open stub, one short stub and three serial lines]

The design-2 SOMI configuration is illustrated in **Figure 5**. The optimized characteristic impedances of design-2 SOMI obtained by PSO, CSA, and GSA. The algorithm steps have discussed in Section 3 by which these characteristic impedances are attained. **Table 8** offers the optimized characteristic impedances of the line elements of Design-2 SOMI. For the frequency response analysis of the design-2 SOMI, the same parameters are selected as the design-1 SOMI as shown in **Figure 6 (a)–(f)**. In **Table 9**, the total magnitude and phase errors are listed. **Table 10** and **Table 11** summarize the statistical analysis and the qualitatively analyzed data of different characteristics of magnitude error of the design-2 SOMI. It is observed that GSA-based results have the least values in all aspects as compared to the PSO and CSA. The pole-zero plot of the Design-2 SOMI for stability analysis in which all the poles and zeros lie inside the unit circle is shown in **Figure 6(d)**. This plot asserts that SOMI Design-2 is stable. The convergence profile of all three algorithms in which GSA is clearly demonstrated to be faster than PSO and CSA with less execution time is shown in **Figure 6(e)**, which is also summarized in **Table 12**. The percentage improvement comparison in magnitude error for the design-2 SOMI as CSA to PSO, GSA to PSO, and GSA to CSA and the percentage improvement comparison in process error, summarized in **Table 13**, are shown in **Figure 6(f)**.



**Figure 5.**  
 Configuration of the design-2 SOMI.

Characteristic impedance	PSO	CSA	GSA
$Z_{OC}$	116	26.87	141
$Z_{TL1}$	30.5	142.6	33
$Z_{TL2}$	145	84	138
$Z_{TL3}$	9.5	19	10
$Z_{SC}$	110	138.09	116.89

**Table 8.**  
 Optimized characteristic impedances of the design-2 SOMI.

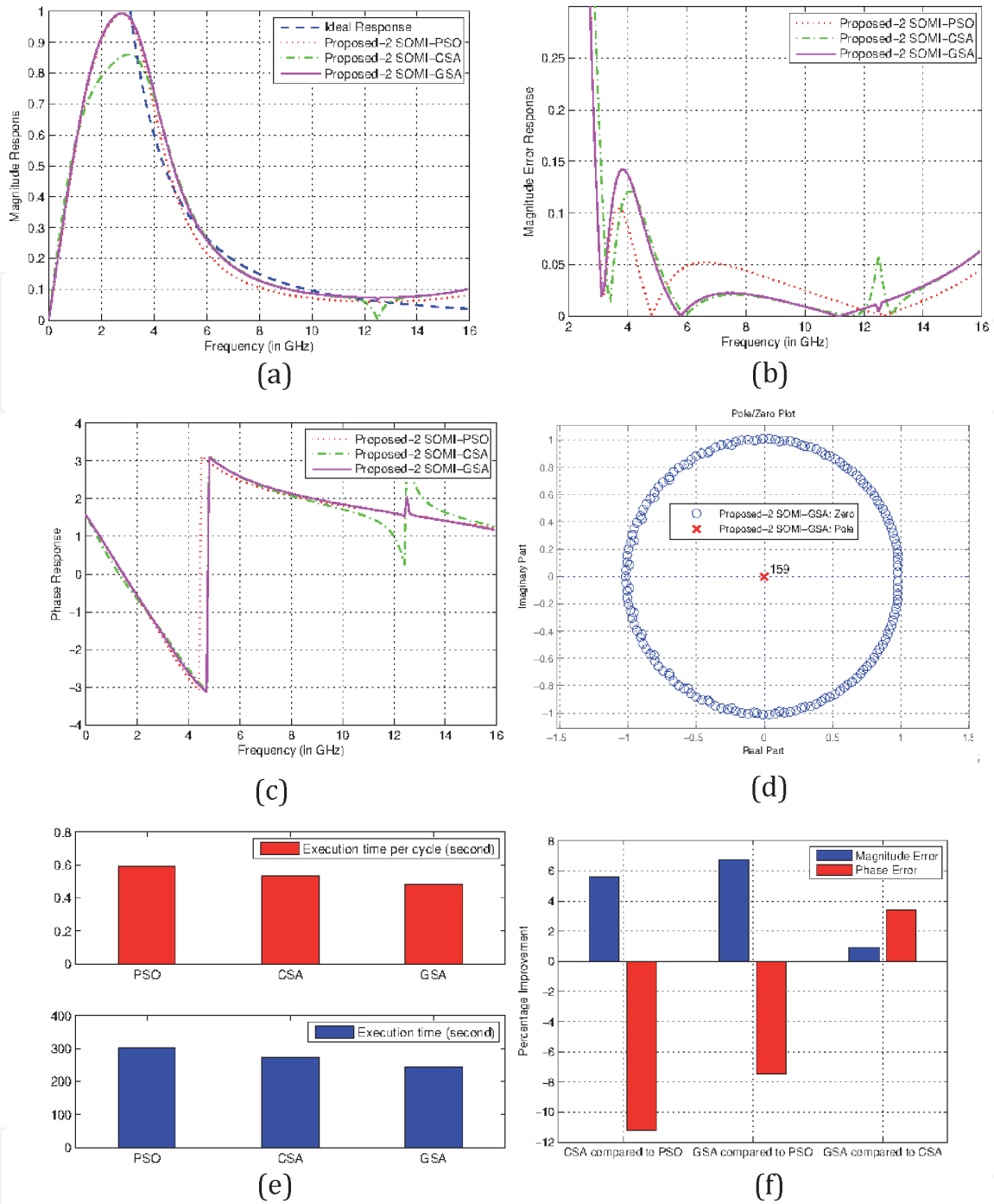


**Figure 6.** Profile of the design-2 SOMI (a) Magnitude response, (b) Magnitude error response, (c) Phase response, (d) Pole-zero plot, (e) Convergence profile, and (f) Improvement bar graph.

Algorithm	Total magnitude error	Phase error
PSO	3.9217	0.9861
CSA	3.6920	1.0968
GSA	3.6573	1.0595

**Table 9.** Comparison summary of total magnitude and phase error for design-2 SOMI.

The Design-2 SOMI GSA-based magnitude response closely matches that of the ideal one in the 3.0–15 GHz frequency range. Based on the observations, compared to PSO and CSA, GSA has the least magnitude error and highest convergence speed.

Algorithm	Mean	Variance	Standard deviation
PSO	0.0324	$5.6118 \times 10^{-4}$	0.0237
CSA	0.0303	0.0013	0.0354
GSA	0.0300	0.0012	0.0343

**Table 10.**  
 Statistical data of magnitude error for design-2 SOMI.

Algorithm	Maximum	Minimum	Average
PSO	0.1048	$2.59 \times 10^{-4}$	0.0324
CSA	0.2097	$9.35 \times 10^{-4}$	0.0303
GSA	0.1425	$3.67 \times 10^{-4}$	0.0300

**Table 11.**  
 Qualitatively data of magnitude error for design-2 SOMI.

Algorithm	Iteration cycle	Execution time (s) per iteration	Execution time (s) per cycle
PSO	400	301.5411	0.5918
CSA	400	273.1862	0.5356
GSA	400	244.6284	0.4802

**Table 12.**  
 Convergence profile for design-2 SOMI.

Algorithm	Magnitude PI (%)	Phase PI (%)
PSO	5.8571	-11.22
CSA	6.7419	-7.443
GSA	0.9398	3.400

**Table 13.**  
 Percentage improvement in magnitude and phase error for design-2 SOMI.

**Figure 7** depicts the comparison of the designed SOMIs with the existing second order microwave integrator. **Figure 7(a)** and **(b)**, respectively, display the comparative magnitude response and AME of the designed SOMI GSA-based optimization with an existing integrator. The corresponding qualitative and statistical magnitude error analysis of the existing SOMIs and the designed integrator is shown in **Table 14**. **Figure 7** and **Table 14** confirm that GSA-based designed SOMIs are more suitable in terms of magnitude, minimal magnitude error, and wide bandwidth, especially for high-frequency ranges.

The results of the proposed-2 SOMI GSA-based leads in performance to the proposed-1 SOMI counterpart. All simulation results of the design-2 SOMI approximates with the ideal one and have linear phase response in its frequency range 3.0–15 GHz. Therefore, the designed-2 SOMI is simulated on ADS by using microstrip lines. To simulate the designed-2 SOMI on ADS, RT/duroid substrate is selected with dielectric constant  $\epsilon_r=2.2$ , height of substrate ( $H$ ) = 30 mil (0.762 mm), loss tangent  $\tan(\delta) = 0.001$ , and copper cladding is 35  $\mu\text{m}$ . The magnitude and phase response of the designed-2 SOMI GSA-based is illustrated in **Figure 8(a)** and **(b)** respectively.



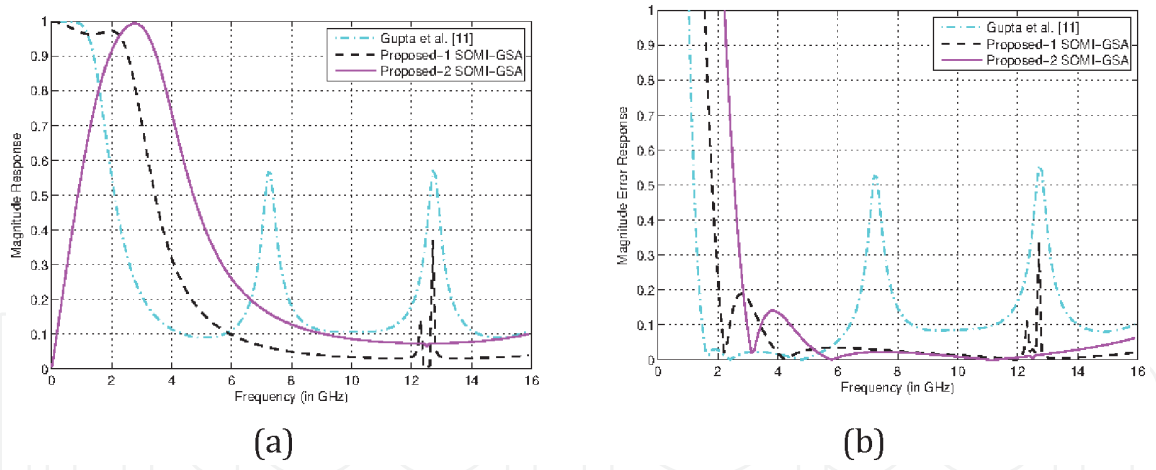


**Figure 7.** Comparison of the designed SOMI-GSA with existing integrator (a) Magnitude response and (b) Error response.

Integrator Order	Frequency range	Reference	Total error	Max error	Min error	Mean error	Variance	Standard deviation
2nd	1–10 GHz	Gupta et al. [11]	10.46	1.11	$1.756 \times 10^{-4}$	0.115	0.0308	0.1755
	1–15 GHz	[11]	17.98	1.11	$1.756 \times 10^{-4}$	0.137	0.0278	0.1667
2nd	2.5–16 GHz	Design-1 SOMI	4.995	0.238	$4.211 \times 10^{-4}$	0.035	0.0024	0.0494
2nd	3–15 GHz	Design-2 SOMI	3.657	0.142	$3.67 \times 10^{-4}$	0.030	0.0012	0.0343

**Table 14.** Comparison of magnitude error of the designed SOMIs with existing design method.

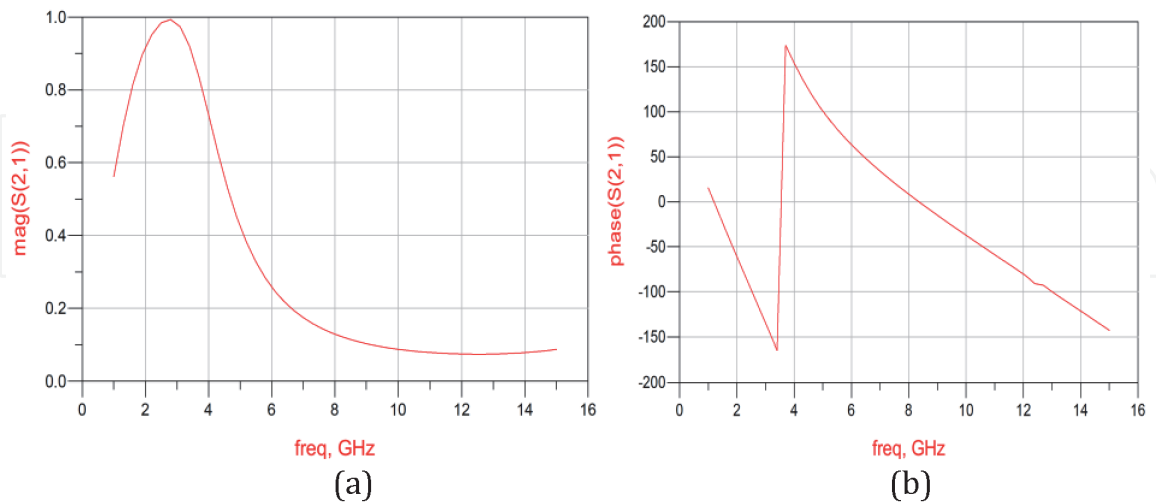


**Figure 8.** Using ADS software (a) Magnitude response and (b) Phase response.

## 5. Conclusion

The study focused on the design and analysis of compact, stable and wideband second order microwave integrators. The designs are obtained by cascading the line


elements i.e. transmission line sections, open-circuited stub and short-circuited stub. The optimum values of line elements are obtained by applying the PSO, CSA and GSA by which the magnitude response of designed integrators approximate the ideal magnitude response. The results are simulated statistically on MATLAB, which affirms that GSA outperforms the PSO and CSA in all state-of-the-art in terms of magnitude response. Furthermore, the designed-2 SOMI GSA-based is also simulated on ADS using microstrip lines. With the exception of lower frequency range (under 3 GHz), the simulated magnitude response of integrator has consistency over the frequency range from 3 to 15 GHz with ideal one in both MATLAB and ADS environment, which makes it appropriate for ultra-wideband applications.

## Author details

Usha Gautam\* and Tarun Kumar Rawat  
Division of Electronics and Communication, Netaji Subhash Institute of  
Technology, Delhi, India

\*Address all correspondence to: [usha.aitpg@gmail.com](mailto:usha.aitpg@gmail.com)

## IntechOpen

© 2021 The Author(s). Licensee IntechOpen. This chapter is distributed under the terms of the Creative Commons Attribution License (<http://creativecommons.org/licenses/by/3.0>), which permits unrestricted use, distribution, and reproduction in any medium, provided the original work is properly cited. 

## References

- [1] Oppenheim AV and Shafer RW: Discrete-Time Signal Processing. New Jersey: Prentice-Hall. 1989.
- [2] Ngo NQ: A new approach for the design of wideband digital integrator and differentiator. IEEE Transactions on Circuits and Systems II: Express Briefs; 2006; 53; 936–940.
- [3] Skolnik MI: Introduction to Radar Systems. New York: McGrawHill. 1980.
- [4] Pozar DM: Microwave Engineering, 3rd ed., Wiley, Singapore, 2005.
- [5] Chiang-Hsue: Design and Implementation of filters using transfer function in the Z Domain. IEEE Trans on Microwave theory and Techniques. May 2001; 49; 5.
- [6] Hsue CW, Tsai LC and Kan ST: Implementation of a trapezoidal rule microwave integrator. Microwave and Optical Technology Letters. 2006; 48; 822–825.
- [7] Hsue C-W, Tsai L-C, Tsai Y-H.: Time-constant control of microwave integrators using transmission lines. IEEE Transactions on Microwave Theory and Techniques. 2006; 54; 1043–1047.
- [8] Tsai L-C and Wu Y-T: Time-constant control analysis of microwave differentiators. IET Microwaves, Antennas & Propagation. 2008; 3; 1044–1050.
- [9] Tsai LC and Fang HS: Design and implementation of second-order microwave integrators. Microwave and Optical Technology Letters. 2011; 53; 1983–1986.
- [10] Gautam U, Upadhyay DK and Rawat TK: New designs of first order microwave integrator. IEEE International Conference on Signal Processing (SPIN), India; 2016 285–289.
- [11] Gupta M and Upadhyay DK: New design of second order microwave integrator. IEEE International Conference on Innovative Mechanisms for Industry Applications (ICIMIA), India; 2017; 556–560.
- [12] Gautam U, Rawat, TK: The optimal design and analysis of wideband second order microwave integrator. International Journal of Microwave and Wireless Technologies. 2019; 11; 3; 227–236.
- [13] Kennedy J and Eberhart R: Particle Swarm optimization. Proceedings of IEEE International Conference Neural Network; 1995; 4; 1942–1948.
- [14] Shi JY and Eberhart RC: Empirical study of particle swarm optimization. Proceedings of the Congress on Evolutionary Computation (CEC99), Washington, DC, USA; 1999; 3; 1945–1950.
- [15] Yang XS and Deb S: Cuckoo search via Levy flights. Proceedings of world congress on nature and biologically inspired computing. USA IEEE Publications. 2009; 210–214.
- [16] Yang XS and Deb S: Cuckoo search: recent advances and applications. Neural Computing & Applications. 2014; 24; 169–174.
- [17] Kumar M and Rawat TK: Optimal fractional delay-IIR filter design using cuckoo search algorithm. ISA Transaction. 2015; 59; 39–54.
- [18] Hong JS and Lancaster MJ: Microstrip Filters for RF/Microwave Applications. New York: Wiley. 2001.
- [19] Rashedi E, Nezamabadi S and Saryazdi S: GSA: a gravitational search algorithm. Information Sciences. 2009; 179; 2232–2248.

[20] Newton Isaac. In *Experimental Philosophy Particular Propositions are Inferred from The Phenomena and Afterwards Rendered General by Induction*, 3rd ed.: Andrew Motte's English Translation published. 1729.

[21] Rashedi E, Nezamabadi S and Saryazdi S: Filter modelling using gravitational search algorithm. *Engineering Applications of Artificial Intelligence's*. 2011; 24; 117–122.

IntechOpen